Deposition of submicron charged particles in turbulent pipe flow with an application to the trachea

H Åkerstedt*

Luleå University of Technology, Department of Engineering
Sciences and Mathematics, Division of Fluid and
Experimental Mechanics, Luleå, Sweden

ABSTRACT

The paper presents a study of the deposition of submicron charged spherical particles caused by convection, Brownian and turbulent diffusion in a pipe with a smooth wall and with a cartilaginous ring wall structure. The model is supposed to describe deposition of charged particles in generation 0 (trachea) of the human respiratory airways. The flow is modeled with a SST-turbulence model combined with a convective-diffusion equation including electric field migration for the particles, and Poisson's equation for the determination of the electrostatic potential in terms of the space-charge density of the particles. An approximate analytical solution is derived for the case of a smooth pipe which is used to verify the numerical solutions obtained from using the commercial software Comsol Multiphysics. Numerical results of deposition rates are also provided for the case of a pipe with a cartilaginous ring wall structure.

1. INTRODUCTION

Studies on particle transport of submicron particles are of high importance in the analysis of particle deposition in the respiratory airways, both for assessing health effects of inhaled toxic matter and for evaluating the efficacy of drug delivery with pharmaceutical aerosols. Transport and deposition in the human lungs can be described in terms of gravitational settling, diffusion, interception, inertial effects and electrostatic effects. Here our focus is on the least studied among these effects the effect of electrostatically charged particles. Both theoretical and experimental studies have demonstrated that electrostatic charge enhances deposition in the lungs, throat, and nasal passages for particles with diameters in the range 0.005–30 µm (Melandri et al.[1,2]). Computational models of the deposition of charged particles in the lung have been developed by Bailey et al.[3,4] and Balachandran et al.[5]. The electrostatic effect on particle deposition was explained either due to space charge effects or image charge forces. The space charge effect is predominant in the upper airways while the image charge effect dominates in the smaller airways.

A more recent theoretical study by Xi et al.[6] consider electrostatic charge effects on pharmaceutical aerosol deposition in the human Nasal-Laryngeal airways. The flow is turbulent and a k-ε turbulence model is applied. The electrostatic effect is treated by using the image charge method so space charge effects are not included. Deposition rates of an order of magnitude larger than no-charge deposition rates were found for particle diameters

_____

*Corresponding Author: hans.akerstedtl@ltu.se

of about 1μm, while lower deposition rates were found for ultra-fine particles. Another recent study by Koullapis et al.[7] considers a realistic air way model from mouth to the end of trachea, simulating the turbulent flow using a LES turbulence model. The effect of electrostatic particles is included using the image charge method. Here it was also found that for particles larger than 1μm the electrostatic effect increases the deposition rate considerably, especially in the mouth-throat region. Studies by Åkerstedt[8] also included the space charge effect for nanoparticles in the lower airways (generation>4) of the human lung in which the flow is laminar. The effect of the wall structure called cartilaginous rings was also included, giving a somewhat smaller deposition.

In the present paper we extend this analysis to charged submicron particles and to the upper airways, especially the first airway called trachea where the flow is usually turbulent. To find the transport and deposition in a given flow geometry there are essentially two methods. A Lagrangian approach and an Eulerian approach. In the Lagrangian approach the equations of motion for each particle are solved including all the forces acting on the particle, the drag force from the fluid, the force by gravity, the force from Brownian motion, electrostatic forces and the force from the fluctuating part of the turbulent motion. For laminar flow and uncharged particles this method has been applied to several studies of the transport of non-spherical particles in the human respiratory airways [9-12]. For the case of charged particles and if only one single particle at a time is launched the force can be calculated by the image force method mentioned above. However if several particles are launched at a time the Coulomb interaction between the particles is also important and since the Coulomb interaction acts over large distance where all particles interact at the same time this is a problem especially since in practice for instance in drug delivery to the human ling the number of particles is huge. Therefore here an Eulerian description is chosen with a space charge distribution of particles related to the particle concentration. The concentration is then governed by a convective diffusion equation including effects from Brownian motion and migration in the self-consistent electric field caused by the charged particles. To include effects from a turbulent flow, turbulent diffusion D_t is added. For particles of size smaller than about one micrometer, turbulent diffusion is the only effect from the turbulence. For larger particles experiments by Liu and Agarwal[13] shows a tremendous increase in deposition for particles beyond diameters around one micrometer. Theoretical models for such large particles including the effect from turbophoresis gives rather good agreement with experiments (Guha[14], Derevich & Zaichik[15]).

From the turbulence point of view this is a more difficult problem to model, since anisotropy near wall effects then become important. This means that the turbulence cannot be modeled by the standard turbulent two-equation models. Here a modification of the $k - \varepsilon$ model that includes the anisotropy near the wall, the $k - \varepsilon - v^2 - f$ model by Durbin[16] can be applied. The paper is organized as follows. In section 2 the set of governing equations of the physical model is introduced, combining the turbulence model equations of the flow with the convective-diffusion equation for the concentration of particles including the migration of charged particles from the electric field. Finally the set of equations is closed by Poisson's equation the equation governing the connection between the space charge density and the electric field.

In section 3 an approximate analytic solution of the model is considered for the case of a smooth pipe and fully developed turbulence. Here an analytic expression for the

deposition rate is derived. This analytic solution is used in section 4 to verify a numerical solution of the model using the commercial software Comsol multiphysics. Finally in section 4 a pipe with a cartilaginous ring structure, supposed to be a model of the trachea of the human lung, is analyzed numerically.
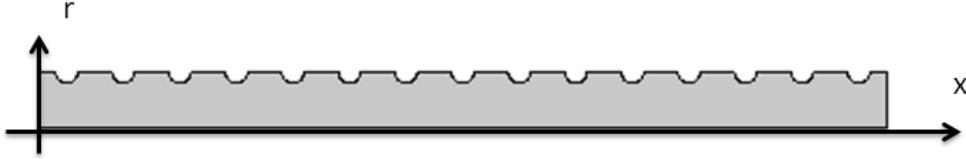

Figure 1. Axisymmetric pipe geometry with a cartilaginous ring wall structure. Radius of Trachea a=0.008[m] length 0.096[m]. Amplitude of rings 0.0008[m].

2. MODEL

The morphology of the respiratory airways of the human lung is represented by a bifurcating system of pipes where each pipe belongs to a certain generation. The uppermost airway (generation0) is a single pipe called trachea. The upper airways have a certain wall structure called cartilaginous rings, located in the upper airways of the lung see figure 1. In this paper we only consider results for this single pipe, the trachea.

For the analysis we assume a pipe with axial symmetry. The main flow is then in the x-direction and r is the coordinate in the radial direction. The flow in trachea is turbulent with a typical Reynolds number ranging from 2000 to 10000.

The fluid flow is then assumed to be modeled with the equations for turbulent viscosity models of the form

$$\rho(\mathbf{u} \cdot \nabla)\mathbf{u} = -\nabla p + \nabla \cdot ((\mu + \mu_t)(\nabla \mathbf{u} + (\nabla \mathbf{u})^T))$$

$$(2.1)$$

$$\nabla \cdot \mathbf{u} = 0$$

Here ρ and p are the density and pressure of the air, $\mathbf{u}$ the fluid velocity, μ the viscosity and μ_t the turbulent viscosity.

The convective-diffusion equation including effects from a concentration c of charged particles with charge q and the electrostatic electric field $\mathbf{E}$ is of the form

$$(\mathbf{u} \cdot \nabla)c + \frac{qD}{\kappa T}\nabla \cdot (c\,\mathbf{E}) - \nabla \cdot ((D + D_t)\nabla c) = 0 \qquad (2.2)$$

where the migration velocity from the electric field is given by

$$\mathbf{v} = \frac{qD}{\kappa T}\mathbf{E} \tag{2.3}$$

Here D is the Brownian diffusion coefficient given by

$$D = \frac{\kappa T\, Cu}{3\pi\mu d}$$

$$Cu = 1 + \frac{\lambda}{d}(2.34 + 1.05\exp(-0.39\frac{d}{\lambda})) \tag{2.4}$$

where Cu is the Cunningham factor which is a correction factor needed to bridge the gap between the continuum limit and the free molecular limit for the flow past a spherical particle. λ is the collision mean free path and d is the particle diameter, κ is Boltzmann's constant and T the temperature.

The turbulent diffusion coefficient is related to the turbulent viscosity as

$$D_t = \frac{\mu_t}{\rho} \tag{2.5}$$

It is also convenient to introduce the dimensionless number α which is here called the electrostatic parameter

$$\alpha = \frac{1}{4}\frac{C_0(0)q^2a^2}{\varepsilon_0\kappa T} \tag{2.6}$$

Here $C_0(0)$ is the concentration at the inlet of the pipe and a the radius of the pipe. The electric field is determined by Poisson's equation with electrostatic potential ϕ

$$\nabla^2\phi = -\frac{qc}{\varepsilon_0} \tag{2.7}$$

which is the equation providing the connection between the space charge distribution and the electrostatic potential.

3. THEORY FOR SMOOTH PIPE

To verify the results of numerical calculations to be presented later using the commercial software Comsol Multiphysics an approximate analytic solution for the deposition of charged particles in a fully-developed turbulent flow in a simple smooth pipe with no cartilaginous rings is considered.

The concentration is then assumed to be uniform across the flow except in a very thin layer close to the boundary. In the main part of the cross section the concentration $C_0(x)$ is assumed

to be a function only of the stream-wise coordinate x. It is assumed to be a weakly varying function of coordinate x, i.e. a boundary layer approximation is assumed. An approximate solution of Poisson's equation disregarding the very thin layer in which the concentration is varying very quickly is then simply

$$\phi(r,x) = \frac{C_0(x)q}{4\varepsilon_0}(a^2 - r^2) \tag{3.1}$$

The wall is considered to be an ideal conductor so the boundary condition for the potential is zero at the wall, which is fulfilled by (3.1). Introduce the dimensionless coordinates $\bar{x} = x/a$ and $\eta = r/a$. In dimensionless units equation (2.2) becomes

$$\bar{u}(\eta)\frac{\partial c}{\partial \bar{x}} + \frac{\alpha}{Pe}C_0(\bar{x})\frac{1}{\eta}\frac{\partial}{\partial \eta}(\eta^2 c) = \frac{1}{Pe}\frac{\partial}{\eta}\frac{\partial}{\partial \eta}(\eta(1+\chi_t(\eta))\frac{\partial c}{\partial \eta}) \tag{3.2}$$

where we have introduced the Peclet numbers Pe,

Pe_t and χ_t defined as

$$Pe = \frac{U_0 a}{D}$$

$$Pe_t = \frac{U_0 a}{D_t}$$

$$\chi_t = \frac{Pe_t}{Pe} \tag{3.3}$$

Here U_o is the mean velocity and the dimensionless velocity $\bar{u}(\eta)$ is defined as

$$\bar{u}(\eta) = \frac{u(\eta)}{U_0} \ . \tag{3.4}$$

For the case of diffusion dominated by Brownian motion the ordinary Peclet number is the relevant dimensionless number in equation (3.2), while in the case of dominating turbulent diffusion the turbulent Peclet number is more relevant. Since both diffusion terms are included in the analysis that follow, the only place where using Pe_t as the relevant dimensionless number is in the estimate of the concentration boundary layer thickness defined below. The concentration c is normalized as

$$C_0(\overline{x}) = C_0(0)\overline{C}_0(\overline{x})$$
$$c(\overline{x},\eta) = C_0(0)\overline{c}(\overline{x},\eta)$$

(3.5)

The limit of large Pe is considered. The diffusion term on the right hand side (3.2) is then important only in a boundary layer close to the wall. Neglecting the diffusion term equation (3.2) becomes

$$\overline{u}(\eta)\frac{\partial \overline{c}}{\partial \overline{x}} + \frac{\alpha}{Pe}C_0(\overline{x})\frac{1}{\eta}\frac{\partial}{\partial \eta}(\eta^2\overline{c}) = 0$$

(3.6)

If $\alpha/Pe \ll 1$ then (3.6) reduces to $\partial \overline{c}/\partial \overline{x} = 0$. Therefore if $\overline{c}$ is uniform except for a small boundary layer at the inlet then $\overline{c}$ is uniform in the main part of the flow. The condition $\partial \overline{c}/\partial \overline{x} = 0$ means that $\overline{c}$ is does not vary over a stream-wise distance of the order of the pipe radius but may vary on a longer length scale X, a scale to be determined from the analysis to follow.

This solution obviously does not satisfy the boundary condition $\overline{c}(\overline{x},0) = 0$ at the wall so therefore a boundary layer analysis treating the behavior near the wall is considered. Introduce a boundary layer coordinate Y

$$Y = (1-\eta)Pe^{v}$$

(3.7)

It is assumed that α is large but α/Pe small so that $\alpha = \overline{\alpha}Pe^{\beta}$ is chosen with $\beta < 1$. Rewriting equation (3.2) in the new coordinate gives

$$\overline{u}(1 - Pe^{-v}Y)\frac{\partial \overline{c}}{\partial \overline{x}} + \frac{\overline{\alpha}Pe^{\beta+v}}{Pe}\overline{C}_0(\overline{x})\frac{\partial \overline{c}}{\partial Y} = Pe^{2v-1}\frac{\partial}{\partial Y}((1+\chi_t)\frac{\partial \overline{c}}{\partial Y})$$

(3.8)

To estimate the first term on the left hand side we use the properties of the turbulent velocity near the wall (Schlichting and Gersten[17]) i.e.

$$u^+ = \frac{u}{u_*} = y^+ + O(y^{+4})$$

$$y^+ = (1-\eta)Re_*$$

$$Re_* = \frac{u_*a}{v}$$

$$Re = \frac{U_0 2a}{v}$$

(3.9)

Equation (3.8) then becomes

$$\frac{2Re_*^2}{Re}Pe^{-\nu}Y\frac{\partial \overline{c}}{\partial \overline{x}} = \frac{\overline{\alpha}Pe^{\beta+\nu}}{Pe}\overline{C}_0(\overline{x})\frac{\partial \overline{c}}{\partial Y} + Pe^{2\nu-1}\frac{\partial}{\partial Y}((1+\chi_t)\frac{\partial \overline{c}}{\partial Y}) \quad (3.10)$$

Balancing the order of magnitude of the terms on the right hand side gives $\nu = \beta$. Since $Re_* \ll Re \ll Pe$, the term on the left hand side can be neglected in the boundary layer and equation (3.10) is then reduced to

$$\overline{\alpha}\overline{C}_0(\overline{x})\frac{\partial \overline{c}}{\partial Y} + \frac{\partial}{\partial Y}((1+\chi_t)\frac{\partial \overline{c}}{\partial Y}) = 0 \quad (3.11)$$

The boundary layer thickness then scales as $O(Pe^{-\beta})$ where $\beta < 1$ or $O(\alpha^{-1})$. The boundary layer thickness without electrostatic effects scales as $O(Pe^{-1/3})$, provided that $Re_*^2/Re \sim O(1)$. So the electrostatic effects lead to thinner boundary layers for $\beta > 1/3$. In the case turbulent diffusion is dominating the estimate of boundary layer thickness should be based upon Pe_t instead of Pe. Integrating (3.11) once gives

$$\overline{\alpha}\overline{C}_0(\overline{x})\overline{c} + (1+\chi_t)\frac{\partial \overline{c}}{\partial Y} = \overline{C}_0(\overline{x})\overline{V}_{dep}(\overline{x}) \quad (3.12)$$

Where

$$\overline{V}_{dep}(\overline{x}) = \frac{V_{dep}(\overline{x})Pe}{U_0 Pe^{\beta}} \quad (3.13)$$

is defined as a dimensionless deposition velocity which is so far an unknown function of $\overline{x}$. Integration of (3.12) leads to the solution

$$\overline{c}(\overline{x},Y) = \frac{\overline{V}_{dep}(\overline{x})}{\overline{\alpha}}(1 - \exp(-\overline{\alpha}\overline{C}_0(\overline{x})\tilde{Z}(Y))) \quad (3.14)$$

where

$$\tilde{Z}(Y) = Pe^{\beta}\overline{Z}(Y) = Pe^{\beta}\int_0^Y \frac{dY}{1+\chi_t(Y)} \quad (3.15)$$

In the limit $Y \to \infty$ the concentration should approach $\overline{C}_0(\overline{x})$, from (3.14) it then follows that

$$\overline{V}_{dep}(\overline{x}) = \frac{\overline{\alpha}\,\overline{C}_0(\overline{x})}{1 - \exp(-\alpha\,\overline{C}_0(\overline{x})\overline{Z}(\infty))} \tag{3.16}$$

To obtain an equation for the development of the mean concentration $\overline{C}_0(\overline{x})$, equation (3.2) is multiplied by η and integrated from zero to unity with the result

$$\int\limits_0^1 \frac{\partial \overline{c}(\overline{x},\eta)}{\partial \overline{x}}\overline{u}(\eta)\eta\,d\eta \;=\; \frac{1}{Pe}\left.\frac{\partial \overline{c}}{\partial \eta}\right|_{\eta=1} = -Pe^{-1}\frac{\alpha\,\overline{C}_0(\overline{x})^2}{1 - \exp(-\alpha\overline{C}_0(\overline{x})\overline{Z}(\infty))} \tag{3.17}$$

Evaluating the left hand side exact analytically is hard but an approximate estimate shows that a good approximation is to take $\overline{c}(\overline{x},\eta)$ uniform in the integral across the flow. Since the concentration $\overline{c}(\overline{x},\eta)$ varies rapidly only in a very thin boundary layer and in which the mean velocity $\overline{u}(\eta)$ is small a rather good approximation to (3.17) is

$$\frac{d\overline{C}_0}{d\overline{x}} = -Pe^{-1}\frac{2\alpha\,\overline{C}_0(\overline{x})^2}{1 - \exp(-\alpha\overline{C}_0(\overline{x})\overline{Z}(\infty))} \tag{3.18}$$

From (3.18) it is noted that the evolution of the mean concentration is on a slow length scale $X = \alpha/Pe\,\overline{x}$ as discussed earlier.

In the integral $\tilde{Z}(\infty) = \int\limits_0^\infty \frac{dY}{1 + \chi_t(Y)}$ where $\chi_t = \nu_t/D$ we use the turbulent viscosity from the indirect turbulence model by Schlichting and Gerstin[17]. However the dominant contribution to the integral comes from the region close to the wall in which the behavior of the turbulent diffusivity is simple given by

$$D_t^+ = \nu_t^+ = \frac{\nu_t}{\nu} \sim A \cdot y^{+3} \quad as \; y^+ \to 0$$

$$A = 6.1 \times 10^{-4} \tag{3.19}$$

The integral can then be evaluated analytically with the result

$$\tilde{Z}(\infty) = Pe^{\beta}\frac{2^{2/3}\sqrt{3}\,\pi}{9\,A^{1/3}Re_*}\left(\frac{Re}{Pe}\right)^{1/3} = Pe^{\beta}\overline{Z}(\infty) \tag{3.20}$$

In the limit of no electrostatic effects $\alpha \to 0$ (3.18) becomes

$$\frac{d\overline{C}_0}{d\overline{x}} = -\frac{2\,\overline{C}_0}{Pe\,\overline{Z}(\infty)} = -\frac{18\,A^{1/3}Re_*}{Pe^{2/3}\,2\sqrt{3}\,\pi Re^{1/3}}\overline{C}_0 \tag{3.21}$$

leading to an exponential decay of concentration on the length scale $O(Pe^{2/3}Re^{1/3}/Re_*)$.

In the opposite limit if α is large such that $\exp(-\alpha\overline{C}_0(\overline{x})\overline{Z}(\infty))$ is small then the development of the mean concentration is governed by the equation

$$\frac{d\overline{C}_0}{d\overline{x}} = -\frac{2\alpha\,\overline{C}_0^2}{Pe} \tag{3.22}$$

leading to a solution of the form

$$\overline{C}_0(\overline{x}) = \frac{1}{1 + \dfrac{2\alpha}{Pe}\,\overline{x}}. \tag{3.23}$$

The amount of deposition $P(\overline{x})$ after a length $\overline{x}$ can now be defined as

$$P(\overline{x}) = 1 - \overline{C}_0(\overline{x}) \tag{3.24}$$

For a short pipe of length $\overline{L}$ an approximate expression for the deposition is

$$P(\overline{L}) = Pe^{-1}\frac{2\alpha\overline{L}}{1 - \exp(-\alpha\overline{Z}(\infty))} \tag{3.25}$$

The conclusion from this theoretical study regarding the electrostatic effect is that deposition is linear in the electrostatic parameter

$$\alpha = \frac{1}{4}\frac{C_0(0)q^2a^2}{\varepsilon_0\kappa T} \tag{3.26}$$

Deposition is thus proportional to concentration at the inlet $C_0(0)$ and quadratic in charge q. The most powerful method to vary deposition is thus varying the charge. A similar

scaling has been found for the case of laminar flow by Yu[18] with a correction later given
by Hashish et al[19]. However Yu does not include effects from Brownian diffusion.

4. COMPARISON BETWEEN THEORETICAL AND NUMERICAL RESULTS

In this section the theoretical results obtained in the previous section are compared with
numerical solutions for the case of a smooth pipe. This means that equations (1.1-1.5) are
solved for a pipe of length 0.12m and radius a=0.008m, which are typical dimensions of the
trachea.

   Especially consider the case of a mean velocity of 4 m/s and particle size ranging from
10nm to 1000nm. The charge of the particles considered range from 0 to 50 elementary
charge units. For the numerical solution we use the commercial software Comsol
Multiphysics 5.2a using the SST-turbulence model for the flow. For the diffusion of
particles we use the Chemical species transport module for the case of diluted species and
for the electrostatics we use the AC/DC module.

   In all the numerical results the mesh is refined until the result becomes independent of
the mesh.

   To compare with the theoretical analysis we choose as velocity field corresponding to a
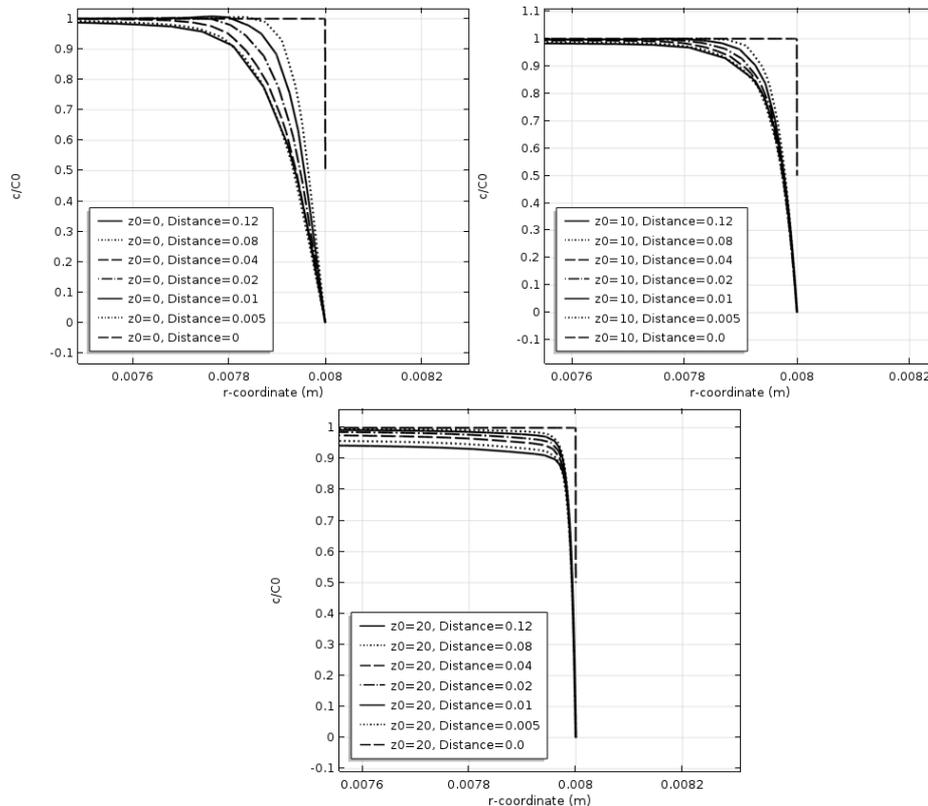fully developed turbulent flow.

Figure. 2. Evolution of concentration boundary layers for different values of the
charge number z0 and particles with diameter 10nm.

In the comparison first consider the development of the concentration distributions for different values for the electrostatic parameter α. The distribution of $\overline{c}$ is chosen uniform at the inlet $\overline{x} = 0$.

The development of the concentration boundary layer is shown in figure 2 for different values of the charge $z0$ corresponding to different values of the electrostatic parameter α. The size of the particles is small equal to 10 nm. The Reynolds number is then Re=4129 and the Peclet number is $Pe = 5.8 \times 10^5$. The influence of the electrostatic particles and fields is clearly observed in which the boundary layer thickness decreases with increasing charge and the electrostatic parameter α. As a second example in figure 3 the corresponding concentration boundary layers are presented for particle diameter 100nm. The Peclet number is then higher $Pe = 4.6 \times 10^7$ leading to even thinner boundary layers. It is also seen that increasing the parameter α leads to thinner layers.
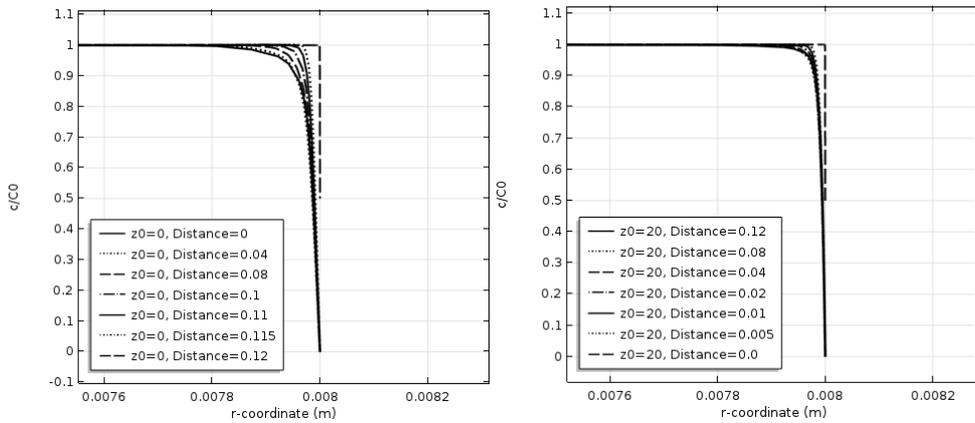

Figure 3. Evolution of concentration boundary layers for different values of the charge number z0 and particle diameter 100nm

For larger particles the boundary layer is very thin especially in the limit of large z0 and α. When comparing the numerically calculated concentration boundary layers with the corresponding boundary layers found from theory there is a difference, the numerical solution gives the evolution of the concentration boundary layer from a uniform distribution at inlet, while the theoretical boundary layer solution cannot cope with a uniform distribution at inlet. The numerical solution however develops very quickly from the initial uniform conditions at inlet. As will be seen however this difference is not so important when considering the corresponding deposition rates.

The fraction of deposited particles after a length L is defined numerically as

$$P_{num}(L) = \frac{-\int_{0}^{L}(D+D_t)\frac{\partial c}{\partial r}\bigg|_{r=a} 2\pi a\, dx}{\int_{0}^{a}(c(0,r)u(0,r)2\pi r dr}$$

(4.1)

Results comparing the theory and the numerical method are shown in figure 4. The theoretical result is calculated from equation (3.25). Results for three different sizes of the particles with diameters 10nm, 100nm and 1000nm are provided. Overall the agreement between theoretical and numerical results is quite good. Some deviation is found for particles with diameter 10nm and large α. The theory was developed for small α/Pe and the value of this parameter for the maximum value of α is around 0.01 which although small nevertheless seems to give some difference. For particles of size 100nm the maximum value of the parameter α/Pe is around 0.001 i.e. much smaller than for 10nm particles and here the agreement between theoretical and numerical results is somewhat better. It should also be noted that there may be some difference in the details of the behavior of the turbulent viscosity for the analytical model and the SST turbulence model close to the wall which also may lead to some difference.
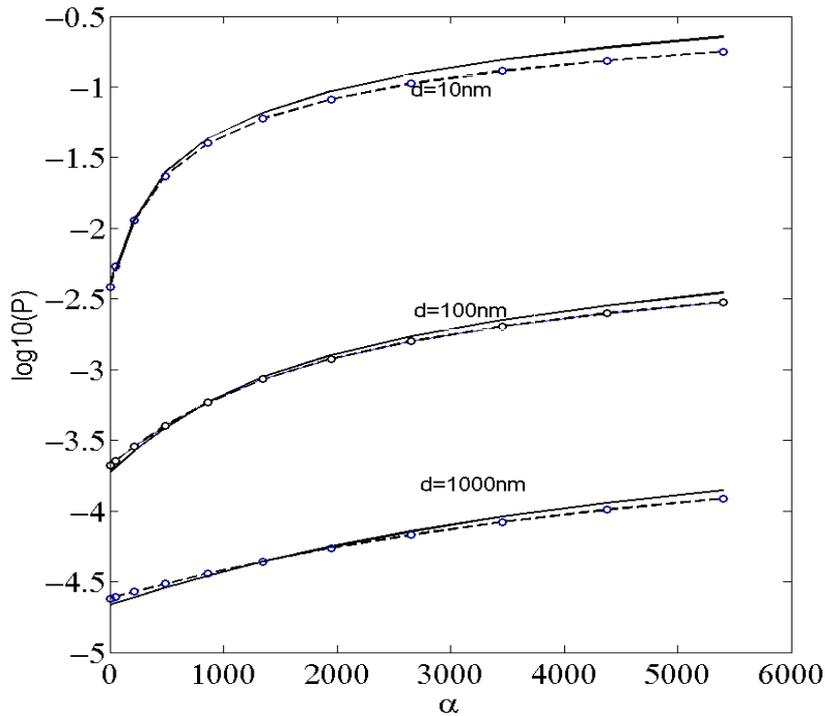

Figure 4. Deposition rate from theory (solid) and numerical calculation (dashed, o) as function of the electrostatic parameter α and for different particle diameters.

Thus for a smooth pipe the theoretical and numerical results overall agree quite well and therefore the theoretical model can be useful for other parameters than presented, especially for prediction of deposition for much larger values of α for which the numerical method is expected to lead to numerical difficulties due to extremely thin boundary layers. The analytical result can then also be applied to the higher generations 1-3 of the human lung.

Since the numerical model also shows good agreement with the theoretical model for a smooth pipe the numerical model is expected to be reliable also for more complex geometries.

In the next section the numerical model will be applied to a pipe with a specific wall structure characterizing the trachea the so called cartilaginous rings. Studies of deposition of charged and uncharged particles in the human lungs with cartilaginous geometry have been conducted in previous studies for the case of laminar flow (Åkerstedt[8]). This is applicable only for the higher generations beyond generation 4. For the first three generations the flow is mainly turbulent.

5. DEPOSITION IN A PIPE WITH CARTILAGINOUS RINGS

Since the numerical method works well for particles with diameters less than about 1μm the method is adopted to a pipe with a cartilaginous ring structure as in figure 1, thus modeling the first generation of the human respiratory airways called the trachea.

The flow parameters are the same as for the smooth pipe with a mean velocity of 4 m/s a pipe diameter of 16mm and a length of 12cm. A difference from the previous section is that here the flow field is chosen uniform at the inlet, i.e. the velocity field is not fully developed as in section 2-3. The amplitude of the rings is chosen as 0.1 of the radius. The typical flow is seen in figures 5a where the flow starts from the top. From the streamlines it is observed that the flow separates in the regions between the rings which may cause some particles to be trapped inside this domain. Of interest is also the electric field line distribution. In figure 5b the electric field lines are shown for the case with particle size 10nm and electrostatic parameter $\alpha=216$. The electric field is stronger at the position of the rings leading to locally larger deposition. Considering the concentration field in figure 5c the concentration boundary layers are extremely thin and are not clearly visible.

In figure 6 the effect of the cartilaginous rings on the amount of deposited particles is presented together with the deposition for the case of a smooth pipe. Comparing figure 6 and 4 for the smooth pipe case there is a slight difference in deposition rates especially for the larger particles of 1000nm. This difference comes from the fully developed velocity profile assumed for the data in figure 4 and the developing flow assumption used for the data in figure 6. Considering the effect of the cartilaginous rings there is a considerable increase in deposition for small values of the electrostatic parameter. For large values the effect of the rings is smaller and seems to approach the result with no rings.
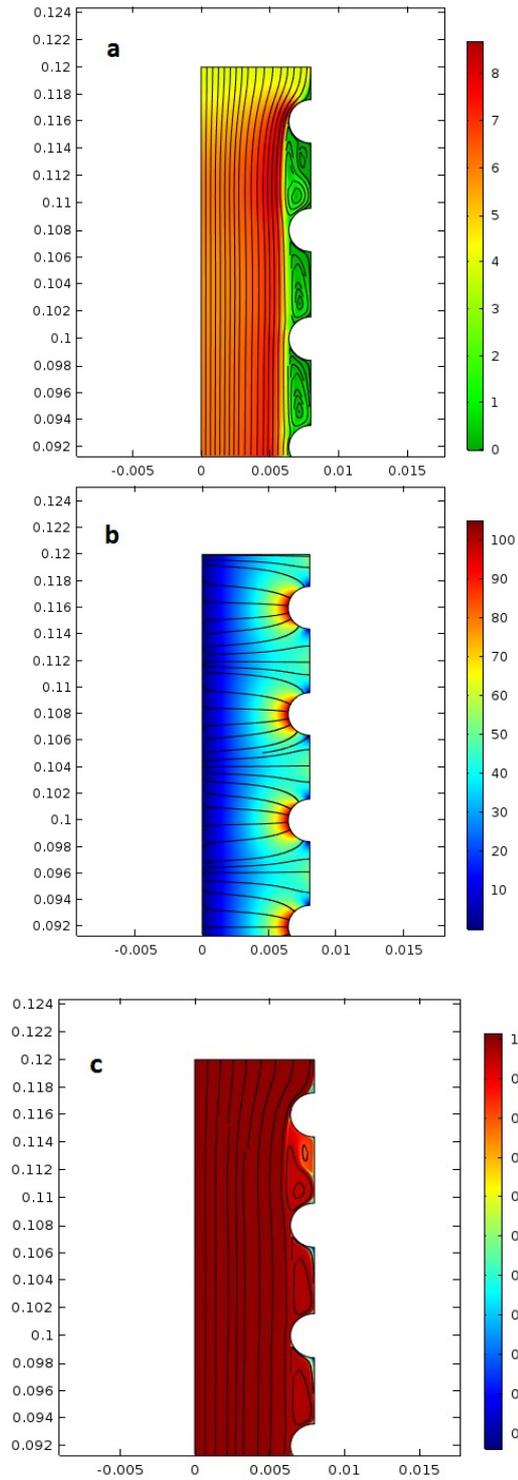
Figure 5. a) Streamlines with color bar indicating velocity magnitude , b) Electric
field lines and color bar indicating electric field magnitude, c) Streamlines with
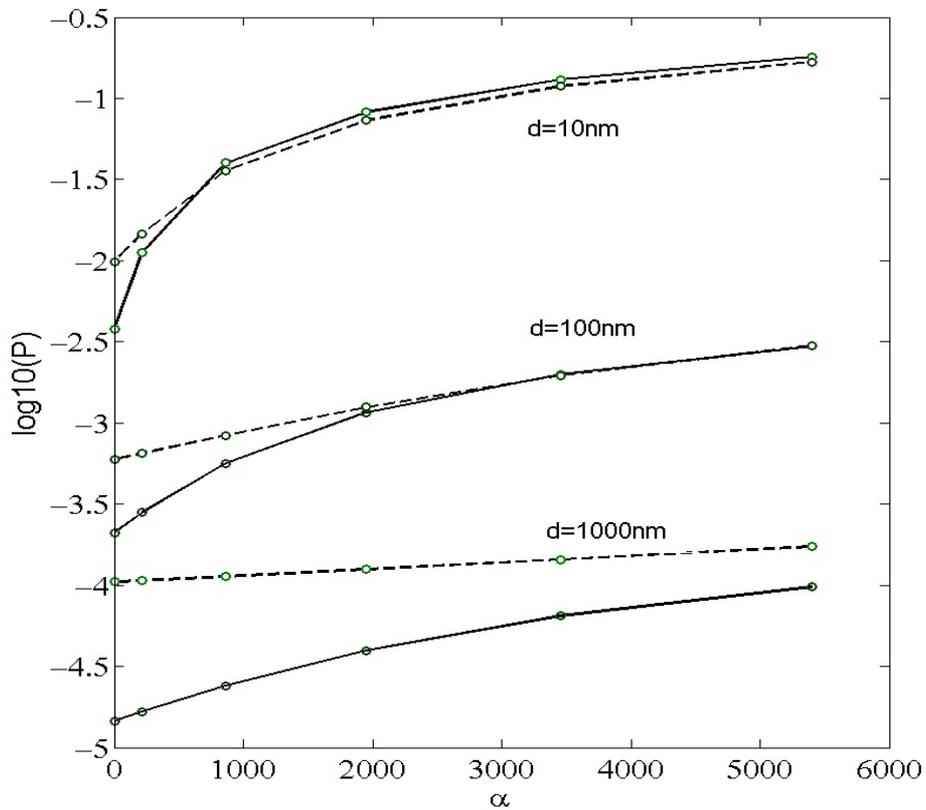color bar indicating concentration

Figure 6. Deposition rate for a smooth pipe (solid) and for a pipe with ring structure (dashed) for different values of the electrostatic parameter

6. CONCLUSION

The paper addresses the effect of space charge distribution of particles on the deposition in a turbulent flow with a smooth wall and a pipe with a wall structure. For the case of a smooth pipe and fully developed flow an approximate analytic solution is presented. The analytical solution is used to verify a numerical solution using the commercial software Comsol Multiphysics. The numerical model includes a combination of an SST-turbulence model for the flow, a convective diffusion equation including migration in electric field for the charged particles and Poissons equation modeling the connection with the space charge density and the electrostatic potential.

The study is restricted to particles smaller than the order of one micrometer. Brownian and turbulent diffusion are included and for smaller particles Brownian diffusion dominates while for larger particles turbulent diffusion becomes more important. Typically the amount of deposition decreases with the size of the particles with a several orders of magnitude difference between particles with diameter 10nm and 1000nm.

The effect of the electrostatic particles is to create an electric field in which the particles migrate towards the wall. This effect may increase deposition by orders of magnitude. Generally it is found that the deposition depends on the electrostatic parameter a parameter which is proportional to concentration of particles at the inlet and proportional to the square of the charge of the particles. From the numerical solution including the effect of the cartilaginous rings there is also an increase in deposition especially for the larger particles. The reason for this is the separation of the flow that occurs between the rings.

The present results are only valid for particles smaller than about one micrometer. Experiments indicate that for particles large than one micrometer there is a several order of magnitude increase in deposition. This effect has been explained by the inclusion of the turbophoresis effect which was mentioned in section 1. In this process particles migrate towards regions with smaller turbulent fluctuations i.e. towards the near wall region. The effect is proportional to the Reynolds stress of the wall normal velocity $\overline{v^{+2}}$ and behaves as $O(y^{+4})$ near the wall. Since other Reynolds stresses for instance $\overline{u^{+2}}$ behaves as $O(y^{+2})$ an anisotropic turbulence model is needed, for instance the $k - \varepsilon - v^2 - f$ model by Durbin mentioned in the introduction. Standard two-equation turbulence models are therefore not useful. The effects of anisotropy, turbophoresis and electrostatic particles on deposition will be considered in future work.

ACKNOWLEDGEMENTS

REFERENCES
[1]   Melandri C, Tarroni G, Prodi V, De Zaiacomo T,Formignani M, Lombardi CC. Deposition of charged particles in the human airways. J Aerosol Sci. 1983;14(5):657-669.

[2]   Melandri C, Prodi V, Tarroni G, et al. On the deposition of unipolarly charged particles in the human respiratory tract. Inhaled Part.1975;4 Pt 1:193-201.

[3]   Bailey A. The inhalation and deposition of charged particles within the human lung. J Electrostatics. 1997;42(1):25-32.

[4]   Bailey A, Hashish A, Williams T. Drug delivery by inhalation of charged particles.J Electrostatics. 1998;44(1):3-10.

[5]   Balachandran W, Machowski W, Gaura E, Hudson C. Control of drug aerosol in human airways using electrostatic forces. J Electrostatics.1997;40–41:579-584.

[6]   Xi J, Si X, Longest W. Electrostatic charge effects on pharmaceutical aerosol deposition in human Nasal–Laryngeal airways. Pharmaceutics. 2014;6(1):26-35.

[7]   Koullapis PG, Kassinos SC, Bivolarova MP,Melikov AK. Particle deposition in a realistic geometry of the human conducting airways: Effects of inlet velocity profile, inhalation flow rate and electrostatic charge. J Biomech.

[8]   Åkerstedt,H.O., Deposition of charged nanoparticles in the human airways including effects from cartilaginous rings. NaturalScience. Vol3,No.10,884-88,(2011)

[9]   Högberg SM, Åkerstedt HO, Lundström TS, Freund JB. Respiratory deposition of fibers in the non-inertial Regime: Development and application of a semi-analytical model. Aerosol Science and Technology. 2010;44(10):847-860

[10]   Högberg SM, Åkerstedt HO, Holmstedt E, Staffan Lundström T, Sandström T. Time-dependent deposition of micro- and nanofibers in straight model airways. Journal of Fluids Engineering. 2012;134(5):051208-051208.

[11]   Åkerstedt, H.O., Högberg, S.M., Lundström,T.S. An asymptotic approach of Brownian deposition of nanofibres in pipe flow. Theor. Comput. Fluid Dyn.

[12]   Holmstedt E, Åkerstedt HO, Lundström TS, Högberg SM. Modelling transport and deposition efficiency of oblate and prolate nano- and micro-particles in a virtual model of the human airway. Journal of Fluids Engineering. 2016.

[13]   Liu, B.Y.H.& Agarwal, J.K. Experimental observation of aerosol deposition in turbulent flow. Aerosol Sci. 1974,5,145-155

[14]   Guha A.Transport and deposition of particles in turbulent and laminar flow. Ann Rev of Fluid Mech. 2008.

[15]   Derevich, I.V.& Zaichik, L.I. Particle deposition from a turbulent flow. Translated from Izvestiya Akademii Nauk SSSR, Mekhanika Zhidkosti I Gaza, No.5, pp.96-104, September-October 1988.

[16]   Durbin PA. Near-wall turbulence closure modeling without "damping functions". Theor Comput Fluid Dyn. 1991;3(1):1-13.

[17]   Schlichting H, Gersten,K. Boundary-layer theory. 8th edition, Springer (2000)

[18]   Yu C. P. Precipitation of unipolarly charged particles in cylindrical and spherical vessels. J Aerosol Sci.1977,8,237-41

[19]   Hashish A.H., Bailey A.G., Williams T.J. Modelling the effect of charge on selective deposition of particles in a diseased lung using aerosol boli. Phys.Med.Biol. 39 (1994) 2247-2262